Two-Dimensional Structural Motif in Thienoacene Semiconductors: Synthesis, Structure, and Properties of Tetrathienoanthracene Isomers

Jaclyn L. Brusso,[†] Oliver D. Hirst,[†] Afshin Dadvand,[†,‡] Srinivasan Ganesan,[†] Fabio Cicoira,[‡] Craig M. Robertson,[§] Richard T. Oakley,[§] Federico Rosei,[‡] and Dmitrii F. Perepichka[†,*]

Department of Chemistry, McGill University, Montreal, Quebec H3A 2K6, Canada, Centre Énergie, Matériaux et Télécommunications, Institut National de la Reserche Scientifique, Varennes, Quebec J3X 1S2, Canada, and Department of Chemistry, University of Waterloo, Waterloo, Ontario N2L 3G1, Canada

Received October 25, 2007. Revised Manuscript Received January 18, 2008

Stille coupling of 2- and 3-(tributylstannyl)thiophene derivatives with tetrabromobenzene followed by oxidative cyclization provides a simple, two-step synthetic route to two isomeric tetrathienoanthracene structures (**13** and **14**). The materials are characterized by a remarkable thermal stability, both in air (T_{dec} $\approx$ 400 °C) and under nitrogen (sublimed with no decomposition at 450–500 °C). Optical studies of the parent and alkylated compounds showed sky-blue photoluminescence with quantum yields ranging between 0.17 and 0.40 and Stokes shifts of 0.03–0.16 eV. Both the optical properties and electrochemical behavior depend strongly on the position of the heteroatoms. Structural studies with X-ray crystallography (for 3D single crystals) and scanning tunneling microscopy (for 2D monolayers) indicate a high level of order, with similar intermolecular interactions for both isomers. The alkylated materials **13b** and **14b** have been used to fabricate thin-film transistors by both vacuum evaporation and solution processing. The preliminary studies show (unoptimized) hole mobilities of up to 7.4×10^{-2} cm^2 V^{-1} s^{-1} and very high on/off ratios of up to 1×10^8 for vacuum-deposited films. The isomer **13**, which showed higher thermodynamic stability of the radical cation and stronger intermolecular S···S contacts, also revealed better device performance.

Introduction

For more than 50 years, the mainstream electronics industry has been dominated by thin film transistors based on inorganic semiconductors such as silicon and gallium arsenide. The fabrication of these devices requires high temperature and high vacuum deposition techniques, which results in high production costs and is particularly prohibitive for large-area electronics. Organic semiconducting materials (OSCs) offer an attractive alternative because their fabrication processes are much less complex compared to conventional inorganic technology.[1] In particular, low-temperature deposition and solution processing techniques provide a simple, low cost alternative. π-Conjugated organic semiconductors are therefore attracting considerable attention for applications such as organic light-emitting diodes (OLEDs), field-effect transistors (OFETs), and photovoltaic cells.[1–4] Furthermore, the flexibility of organic compounds coupled with their low-temperature solution processing provides the potential for new applications including flexible displays, pliable electronic paper and smart cards.[2] While molecular and polymer OLEDs have already been commercialized in a number of consumer products, OLED displays still employ an inorganic (amorphous silicon, a-Si) thin-film transistor (TFT) matrix to control the emissive pixels.[5] Organic TFTs (OTFTs) are nevertheless extensively investigated by a number of industrial and academic groups. The mobility of the best OSCs have already approached and even surpassed that of a-Si ($\sim$1 cm^2 V^{-1} s^{-1}), but to the best of our knowledge, no commercial applications of OTFTs have yet been announced. The limited stability of OSCs and the "difficult to control" molecular packing, particularly in solution-processed devices, are among the major limitations hampering industrial development, and the design of new OSCs continues to be an important area of materials research.

Conjugated oligomers and fused aromatics have attracted considerable attention as the most viable materials for

* Corresponding author. E-mail: dmitrii.perepichka@mcgill.ca.
† McGill University.
‡ Institut National de la Reserche Scientifique.
§ University of Waterloo.

(1) (a) Reese, C.; Roberts, M.; Ling, M.; Bao, Z. *Mater. Today* **2004**, *7*, 20. (b) Dimitrakopoulos, C. D.; Malenfant, P. R. L. *Adv. Mater.* **2002**, *14*, 99. (c) Horowitz, G. *Adv. Mater.* **1998**, *10*, 365. (d) Katz, H. E.; Bao, Z. *J. Phys. Chem. B* **2000**, *104*, 671. (e) Dimitrakopoulos, C. D.; Malenfant, P. R. L. *Adv. Mater.* **2002**, *14*, 99. (f) Sun, Y.; Liu, Y.; Zhu, D. *J. Mater. Chem.* **2004**, *14*, 53.

(2) (a) Reese, C.; Bao, Z. *Mater. Today* **2007**, *10*, 20. (b) Facchetti, A. *Mater. Today* **2007**, *10*, 28. (c) Anthony, J. E. *Chem. Rev.* **2006**, *106*, 5028.

(3) Perepichka,D. F.; Perepichka, I. F.; Meng, H.; Wudl, F. Light-Emitting Polymers. In *Organic Light-Emitting Diodes*; Li, Z. R., Ed.; CRC Press: Boca Raton, FL, 2006.

(4) Williams, E. L.; Haavisto, K.; Li, J.; Jabbour, G. E. *Adv. Mater.* **2007**, *19*, 197.

(5) (a) Kumar, A.; Nathan, A.; Jabbour, G. E. *IEEE Trans. Electron Devices* **2005**, *52*, 2386. (b) Kumar, A.; Sakariya, K.; Servati, P.; Alexander, S.; Striakhilev, D.; Karim, K. S.; Nathan, A.; Hack, M.; Williams, E.; Jabbour, G. E. *IEEE Proc.: Circuits, Devices Syst.* **2003**, *150*, 322.

10.1021/cm7030653 CCC: $40.75
Published on Web 03/07/2008

Chart 1

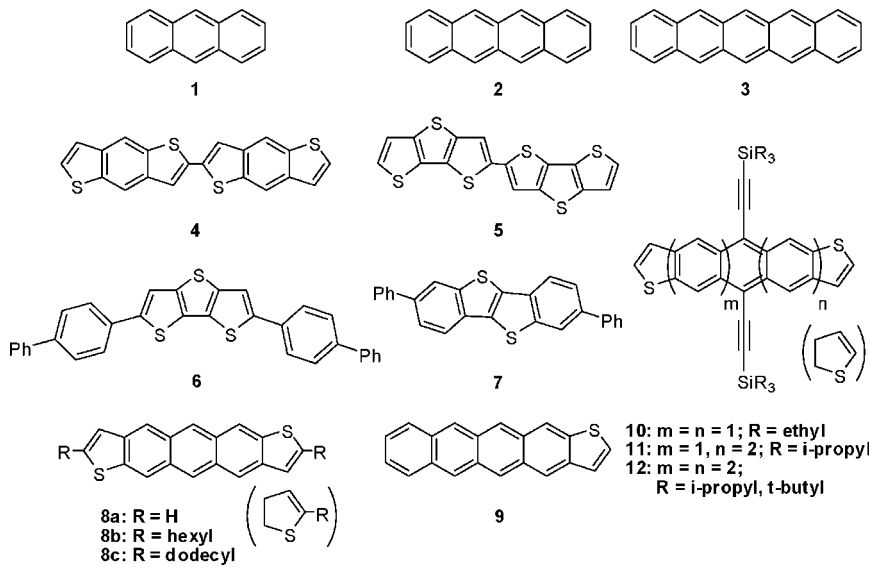

OTFTs. Among these, linear acenes and oligothiophenes are the two most studied classes of OSCs to date.[1,2,6] The charge carrier mobility in organic materials generally increases with the extension of conjugation. For example, hole mobilities (μ_h) of 0.12 and 3.0 $cm^2\ V^{-1}\ s^{-1}$ have been reported for thin films of tetracene (**2**)[7] and pentacene (**3**),[8] respectively (Chart 1). While no discernible mobility has been observed for thin films of anthracene (**1**), single-crystal FET devices have been reported with hole mobility of 0.02 $cm^2\ V^{-1}\ s^{-1}$.[9] Unfortunately, an increased conjugation length is often associated with decreased stability, predominantly because of the significantly raised HOMO in these molecules. It is interesting to mention that in aromatic hydrocarbon OSCs, the change of the connection between the benzene ring from linear (oligophenylenes) to fused (oligoacenes) structure results in a substantial increase in conjugation and charge carrier mobility, with concomitant chemical instability, particularly toward oxidation.[10] Thus, pentacene, the current benchmark semiconductor for OTFTs, is a very reactive molecule such that nonencapsulated devices should be measured and even stored under inert atmosphere to avoid degradation. At the same time, fused thiophene oligomers seem to enjoy an increased stability in comparison with linearly linked structures, together with a more efficient conjugation.[11] In recognition of this fact, a significant focus in organic materials research was lately given to synthesis and device studies of fused thienothiophene and benzothiophene derivatives. Bis(dithienobenzene) **4** represents one of the earliest reports of an air stable organic semiconductor which exhibited reasonable thin film mobility (0.04 $cm^2\ V^{-1}\ s^{-1}$).[12] Similar results were obtained from the fully heterocyclic bis(dithienothiophene) **5** in which thin film devices exhibited mobilities of 0.05 $cm^2\ V^{-1}\ s^{-1}$.[13] More recently, remarkable thin-film mobilities of $\mu_h = 0.4$ $cm^2\ V^{-1}\ s^{-1}$ and even $\sim$2.0 $cm^2V^{-1}s^{-1}$ for related diphenyl(dithienothiophene) **6**[14] and diphenyl(dibenzothienothiophene) **7**,[15] respectively, have been reported.

Combining thiophene and oligoacene building blocks has been another extensively studied approach in design of OSCs. Substantial hole mobilities in OTFT devices have been demonstrated for a series of dithienoanthracenes **8** ($\mu_h \approx 10^{-1}$ $cm^2\ V^{-1}\ s^{-1}$),[16] monothienotetracenes **9** ($\mu_h \approx 1 \times 10^{-1}$ $cm^2\ V^{-1}\ s^{-1}$),[17] and trialkylsilyl acetylene functionalized dithienoanthracenes **10** ($\mu_h \approx 1.0$ $cm^2\ V^{-1}\ s^{-1}$).[18] However, further extension of the conjugation, as in dithienotetracene **11**, resulted in rather low mobility ($\mu_h \approx 1 \times 10^{-5}$ $cm^2\ V^{-1}\ s^{-1}$) and no transistor function was found in dithienopentacene derivatives **12**.[2c,19] Part of the problem with dithienoacene structures **8**, **10**–**12** was that the synthetic approach inevitably led to a statistical mixture of anti and syn- isomers. The difficulties in separation of these isomers, together with the reduced stability for longer dithienoacenes, might well be responsible for the poor performance of **11** and **12** in the OTFTs.

(6) (a) Facchetti, A.; Yoon, M.-H.; Stern, C. L.; Hutchison, G. R.; Ratner, M. A.; Marks, T. J. *J. Am. Chem. Soc.* **2004**, *126*, 13480. (b) Wang, Z.; Kim, C.; Facchetti, A.; Marks, T. *J. Am. Chem. Soc.* **2007**, *129*, 13362.
(7) Gundlach, D. J.; Nichols, J. A.; Zhou, L.; Jackson, T. N. *Appl. Phys. Lett.* **2002**, *16*, 2925.
(8) Kelley, T. W.; Boardman, L. D.; Dunbar, T. D.; Muyres, D. V.; Pellerite, M. J.; Smith, T. P. *J. Phys. Chem. B* **2003**, *107*, 5877.
(9) Aleshin, A. N.; Lee, J. Y.; Chu, S. W.; Kim, J. S.; Park, Y. W. *Appl. Phys. Lett.* **2004**, *84*, 5383.
(10) Reddy, A. R.; Bendikov, M. *Chem. Commun.* **2006**, 1179.
(11) (a) Lee, K.; Sotzing, G. A. *Macromolecules* **2001**, *34*, 5746. (b) Lee, K.; Yavuz, M. S.; Sotzing, G. A. *Macromolecules* **2006**, *39*, 3118.
(12) Laquindanum, J. G.; Katz, H. E.; Lovinger, A. J.; Dodabalapur, A. *Adv. Mater.* **1997**, *9*, 36.
(13) Li, X. C.; Sirringhaus, H.; Garnier, F.; Holmes, A. B.; Moratti, S. C.; Feeder, N.; Clegg, W.; Teat, S. J.; Friend, R. H. *J. Am. Chem. Soc.* **1998**, *120*, 2206.
(14) Sun, Y.; Ma, Y.; Liu, Y.; Lin, Y.; Wang, Z.; Wang, Y.; Di, C.; Xiao, K.; Chen, X.; Qiu, W.; Zhang, B.; Yu, G.; Hu, W.; Zhu, D. *Adv. Funct. Mater.* **2006**, *16*, 426.
(15) Takimiya, K.; Ebata, H.; Sakamoto, K.; Izawa, T.; Otsubo, T.; Kunugi, Y. *J. Am. Chem. Soc.* **2006**, *128*, 12604.
(16) Laquindanum, J. G.; Katz, H. E.; Lovinger, A. J. *J. Am. Chem. Soc.,* **1998**, *120*, 664.
(17) (a) Tang, M. L.; Okamoto, T.; Bao, Z. *J. Am. Chem. Soc.,* **2006**, *128*, 16002. (b) Valiyev, F.; Hu, W.; Chen, H.; Kuo, M.; Chao, I.; Tao, Y. *Chem. Mater.* **2007**, *19*, 3018.
(18) Payne, M. M.; Parkin, S. R.; Anthony, J. E.; Kuo, C. C.; Jackson, T. N. *J. Am. Chem. Soc.* **2005**, *127*, 4986.
(19) Payne, M. M.; Odom, S. A.; Parkin, S. R.; Anthony, J. E. *Org. Lett.* **2004**, *6*, 3325.

Chart 2

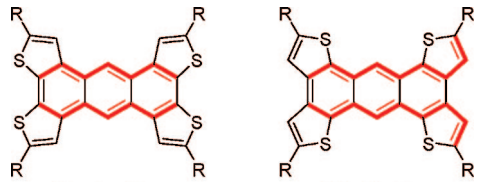

In most cases, modulation of the conjugation in OSC molecules was attained through a linear (1D) elongation of the molecule. Much less is known about the effect of the 2D conjugation extension on the properties of molecular semiconductors. One could expect that for 2D aromatic molecules, the packing in the solid state should favor $\pi\cdots\pi$ stacks vs $\pi\cdots$H−C herringbone packing, common for linear oligoacene and thiophene oligomers.[2c,20] Important examples of such molecules include hexa-peri-hexabenzocoronenes,[21] supertriphenylene,[22] phthalocyanines,[23] and more recently, perylo[1,12-b,c,d]thiophene.[24] However, in contrast to 1D conjugated OSCs, the structure–property relationships and solid-state packing tendencies are much less clear.

In this work, we set to answer some of these questions through studies of the fused heteroaromatic isomers **13** and **14** (Chart 2). It was of particular interest to see if and how the position of a heteroatom in the heteroacene structure (**13** vs **14**) affects the molecular properties and solid-state packing. Specifically, we report the preparation of two isomeric parent tetrathienoanthracenenes **13a** and **14a** and their hexylated derivatives **13b** and **14b**, as highly stable materials with pronounced semiconducting properties. The comparative studies of their electronic properties by cyclic and differential pulse voltammetry, and by UV–visible and fluorescence spectroscopy reveal an important role of the position of the sulfur atoms. The supramolecular organization has been explored in 2D monolayers by scanning tunneling microscopy (STM) and in 3D molecular crystals by X-ray crystallography. We also report our preliminary studies of OTFTs of the two isomeric hexylated compounds **13b** and **14b**. During the preparation of this manuscript, the compound **14b** and its FET devices were reported by Pei et al.[25]

Results and Discussion

Synthesis. Our approach to tetrathienoanthracenes **13** and **14** was based on early work by Tovar, Rose, and Swager who used oxidative cyclization to access a series of dithienonaphthalene derivatives.[26] The 3-[2,4,5-tri(3-thienyl)phenyl]thiophene **16a** was obtained by Stille coupling of 3-(tributylstannyl)thiophene **15**[27] with 1,2,4,5-tetrabromobenzene in DMF at 130 °C in 86% yield (Scheme 1). Attempts at photooxidative cyclization of **16a**, by analogy with synthesis of structurally related thienyl- and phenyl-substituted ethenes,[28] were unsuccessful, generating the intermediate **17** along with an insoluble polymer.[29] However, chemical oxidative cyclization of **16a** with $FeCl_3$ in a dichloromethane (DCM)/nitromethane solution[30] afforded the desired product **13a** in 10% purified yield.

Construction of the isomeric tetrathienoanthracene **14a** (Scheme 2) began in a similar manner with 2-[2,4,5-tri(2-thienyl)phenyl]thiophene **19a** prepared via Stille coupling of 2-(tributylstannyl)thiophene **18** with 1,2,4,5-tetrabro-

Scheme 1[a]

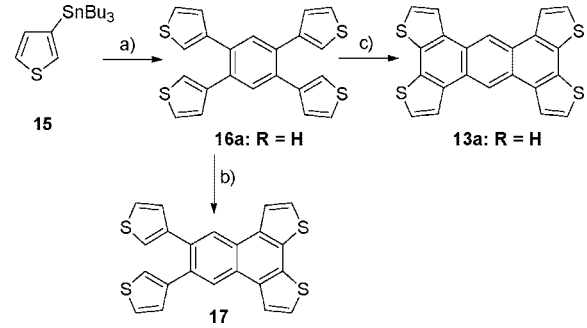

[a] Reagents and Conditions: (a) 1,2,4,5-tetrabromobenzene, $PdCl_2(PPh_3)_2$, DMF, 130 °C; (b) *hν*, O_2, cyclohexane, 10 °C; (c) $FeCl_3$, $MeNO_2$/DCM, RT.

Scheme 2[a]

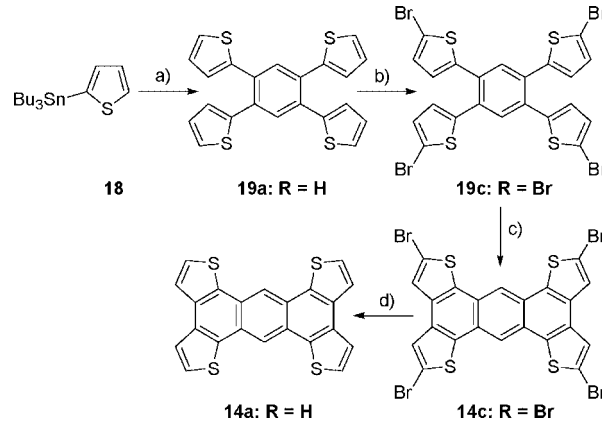

[a] Reagents and conditions: (a) 1,2,4,5-tetrabromobenzene, $PdCl_2(PPh_3)_2$, DMF, 130 °C; (b) NBS, THF, RT; (c) $FeCl_3$, $MeNO_2$/chlorobenzene, RT; d) *t*-BuLi, TMEDA, Ph_2O, 80 °C.

(20) Reese, C.; Bao, Z. *J. Mater. Chem.* **2006**, *16*, 329.
(21) (a) Wu, J.; Baumgarten, M.; Debije, M. G.; Warman, J. M.; Müllen, K. *Angew. Chem., Int. Ed.* **2004**, *43*, 5331. (b) Dou, X.; Yang, X.; Bodwell, G. J.; Wagner, M.; Enkelmann, V.; Müllen, K. *Org. Lett.* **2007**, *9*, 2485.
(22) Iyer, V. S.; Wehmeier, M.; Brand, J. D.; Keegstra, M. A.; Müllen, K. *Angew. Chem., Int. Ed.* **1997**, *36*, 1603.
(23) (a) Schlettwein, D.; Tada, H.; Mashiko, S. *Langmuir* **2000**, *16*, 2872. (b) Ali-Adib, Z.; Clarkson, G. J.; McKeown, N. B.; Treacher, K. E.; Gleeson, H. F.; Stennett, A. S. *J. Mater. Chem.* **1998**, *8*, 2371.
(24) Sun, Y.; Tan, L.; Jiang, S.; Qian, H.; Wang, Z.; Yan, D.; Di, C.; Wang, Y.; Wu, W.; Yu, G.; Yan, S.; Wang, C.; Hu, W.; Liu, Y.; Zhu, D. *J. Am. Chem. Soc.* **2007**, *129*, 1882.
(25) Liu, W.; Zhou, Y.; Ma, Y.; Cao, Y.; Wang, J.; Pei, J. *Org. Lett.* **2007**, *9*, 4187.
(26) Tovar, J. D.; Rose, A.; Swager, T. M. *J. Am. Chem. Soc.* **2002**, *124*, 7762.
(27) Pinhey, J. T.; Roche, E. G. *J. Chem. Soc., Perkin Trans. I* **1988**, *8*, 2415.
(28) Fischer, E.; Larsen, J.; Christensen, J. B.; Fourmigué, M.; Madsen, H. G.; Harrit, N. *J. Org. Chem.* **1996**, *61*, 6997.
(29) Photooxidative cyclization affording a monocyclized product instead of a fully cyclized product has been noted elsewhere. See, for example, Li, Y.; Li, Y.; Li, J.; Li, C.; Liu, X.; Yuan, M.; Liu, H.; Wang, S. *Chem.—Eur. J.* **2006**, *12*, 8378.
(30) Brown, S. P.; Schnell, I.; Brand, J. D.; Müllen, K.; Spiess, H. W. *J. Am. Chem. Soc.* **1999**, *121*, 6712.

Scheme 3[a]

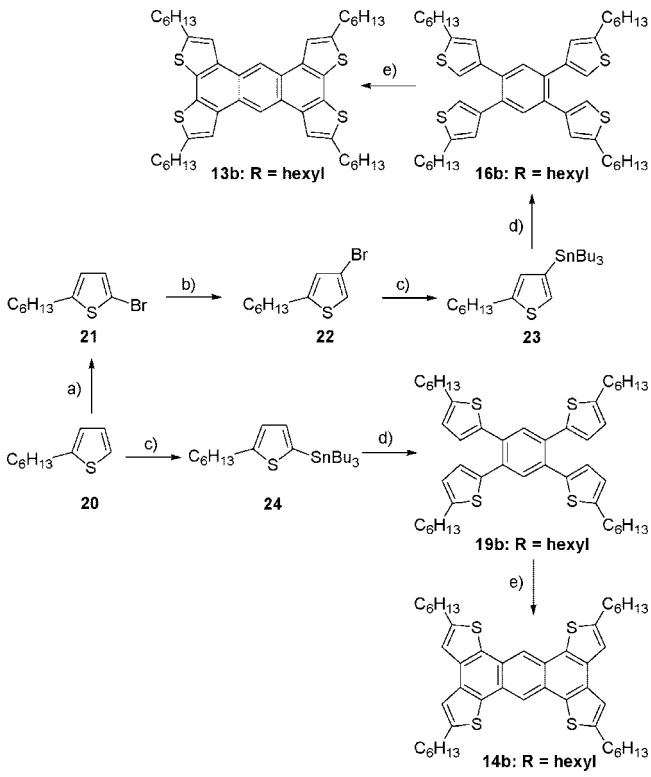

[a] Reagents and conditions: (a) NBS, 2:1 $CHCl_3$:HOAc, RT; (b) LDA, THF, −78 °C; (c) (i) *n*-BuLi, THF, −78 °C; (ii) Bu_3SnCl, −78 °C to RT; (d) 1,2,4,5-tetrabromobenzene, $PdCl_2(PPh_3)_2$, DMF, 130 °C; (e) $FeCl_3$, $MeNO_2$/DCM, RT.

mobenzene. Unfortunately but unsurprisingly, attempts to cyclize **19a**, both chemically and photochemically, did not generate the desired product **14a**, even under high dilution conditions. The known higher spin density of the thiophene radical cation at the 2-position favors the formation of a polymer which was the only observed product. Nevertheless, protection of the thiophene 2-position, via bromination with N-bromosuccinimide (NBS) (to form **19c**) followed by $FeCl_3$ oxidation gave **14c** as a yellow brown solid, practically insoluble in organic solvents. Deprotection of the crude **14c** was carried out in diphenyl ether at 80 °C with *tert*-butyllithium/tetramethylethylenediamine followed by quenching with isopropanol generating the desired parent tetrathienoanthracene **14a** with 44% purified yield. Noteworthy, **14a** is significantly less soluble than its isomer **13a**.

Preparation of the tetrahexyl derivative **13b** required 3-(tributylstannyl)-5-hexylthiophene **23** which was accessed through isomerization of 2-bromo-5-hexylthiophene **21** with LDA[31] followed by lithiation with *n*-butyllithium and treatment with tributyltin chloride (Scheme 3). Stille coupling of **23** with 1,2,4,5-tetrabromobenzene led to **16b**, which was oxidatively cyclized into tetrathienoanthracene **13b** with 91% yield. Its isomer **14b** was prepared in a similar way from 2-(tributylstannyl)-5-hexylthiophene **24**.

Thermogravimetric analysis (TGA) revealed very high stability of compounds **13b** and **14b**, with onset decomposition temperatures (T_{dec}) of ∼400 °C in air. The same

(31) Miguel, L. S.; Porter, W. W.; Matzger, A. J. *Org. Lett.* **2007**, *9*, 1005.

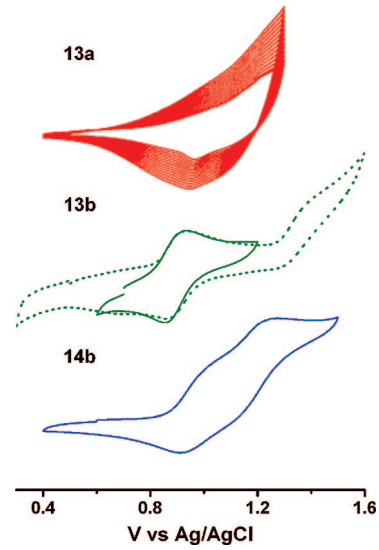

Figure 1. CV scans of **13a** (top, red line), **13b** (middle, green line), and **14b** (bottom, blue line) in DCM with *n*-Bu_4NPF_6 supporting electrolyte.

experiment under nitrogen showed no decomposition until sublimation of the compounds at 450–500 °C (see Supporting Information). Such a remarkable stability (for thiophene derivatives) is particularly important for application of these compounds in OTFTs, where the stability of organic semiconductors is still a major limitation.

Electrochemical and Spectroscopic Studies. The redox properties of tetrathienoanthracenes **13** and **14** were probed by cyclic voltammetry (CV) and differential pulse voltammetry (DPV). Both unsubstituted tetrathienoanthracenes **13a** and **14a** show an irreversible oxidation wave which corresponds to the formation of the radical cation species followed by polymerization. Repeated cycling through the oxidation wave results in growth of a visible polymer film on the electrode (Figure 1). The symmetric arrangement of the linking sites on the monomer unit make it a potential building block for two-dimensional conjugated polymers, and further investigation into the possible formation of ordered polymeric structures is currently underway.

In the case of the substituted tetrathienoanthracenes **13b** and **14b**, blocking the reactive sites prevents electropolymerization and thus reversible waves were observed for these compounds (Figure 1). While initial CV studies of **13b** showed one single electron oxidation, compound **14b** was characterized by two closely spaced oxidation waves with separation of ∼0.3 V, suggesting a sequential formation of a radical cation and a dication. **13b** loses the second electron at much higher potential, at which the second oxidation wave is only partially reversible (Figure 1, green dotted line). To find the exact thermodynamic potentials of the overlapping redox waves, we performed differential pulse voltammetry (DPV) experiments. Two oxidation waves at 0.95 and 1.23 V for **14b** and 0.91 and 1.46 V for **13b** were found (see Table 1 and the Supporting Information). The separation between the first and the second oxidation waves reflects the thermodynamic stability of the radical cation: $E_{½}^{1ox} - E_{½}^{2ox} = -0.059 \log K_{dispr}$.[32] The higher stability of $\mathbf{13b}^{\cdot+}$ ($K_{dispr} = 5 \times 10^{-10}$) as compared to $\mathbf{14b}^{\cdot+}$ ($K_{dispr} = 3 \times 10^{-5}$) is expected to suppress the possible polaron–bipolaron

Table 1. Theoretical,[a] Electrochemical,[b] and Photophysical Properties for 13 and 14

	13a	13b	14a	14b
E_{HOMO}^{calcd} (eV)	−5.18	−4.83[g]	−5.23	−4.92[g]
E_g^{calcd} (eV)	3.52	3.37[g]	3.50	3.40[g]
$E_{½}^{1ox}$ (V)	1.22[h]	0.91	1.69[h]	0.95[i]
$E_{½}^{2ox}$ (V)		1.46[h,i]		1.23[i]
E_{HOMO}^{exp} (eV)	−6.22	−5.91	−6.69	−5.95
λ_{max}^{abs} (nm)[c]	379	405	418	428
λ_{max}^{abs} (nm)[d]		414		437
E_g^{opt} (eV)[e]	3.27	3.06	2.97	2.90
λ_{max}^{PL} (nm)[f]	398	421	422	436
λ_{max}^{PL} (nm)[d]		485		505
Φ_{fl} (%)[50]	17[j]	26[j]	32[k]	40[k]
Stokes shift (eV)	0.16	0.12	0.03	0.05

[a] DFT/B3LYP/6–31G(2d,p) level of theory. [b] In DCM, 0.1 M nBu$_4$NPF$_6$ as supporting electrolyte, and referenced to Ag/AgCl. [c] In DCM. [d] Thin films prepared by drop-casting of chlorobenzene solutions. [e] Calculated from λ_{max} of the longest wavelength transition in the absorption spectrum. [f] In DCM, upon excitation at 370 nm for **13** and 324 nm for **14**. [g] Calculated for R = Me. [h] Irreversible behavior, E_{pa} value quoted. [i] Values obtained from DPV studies. [j] In DCM, 9,10-diphenylanthracene (Φ_{fl} = 90%)[51] as the standard. [k] In cyclohexane, anthracene as the standard (Φ_{fl} = 36%).[52]

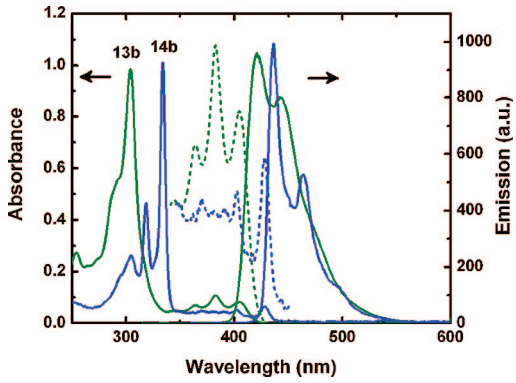

Figure 2. Absorption and emission spectra of **13b** (green line) and **14b** (blue line). The long-wavelength region of the absorbance spectra is shown enlarged (×10, dashed lines).

disproportionation in devices and could result in higher charge mobility.

UV–vis spectra of DCM solutions of **13** and **14** reveal a strong absorption band at ~300–350 nm and a weaker band at ~350–450 nm, both with pronounced vibronic structure characteristic of rigid acene molecules (Table 1 and Figure 2). Introduction of alkyl substituents results in a small bathochromic shift of ~6–7 nm. A larger bathochromic shift of ~30 nm is observed between the isomeric structures **13** and **14** (where R = H or hexyl) which is attributed to longer "effective conjugation" of **14** vs **13**. Indeed, the electronic structure of oligoacenes, although having many features of an aromatic system, can also be represented as two bridged polyene chains.[33] Thus, fusion of the thiophene units to anthracene as in **14** extends the conjugation by two double bonds, while in **13** the conjugation formally is only extended by the lone pairs of the sulfur atoms (shown as red bold lines in Chart 2). While this is certainly an oversimplified approach, the expected trend is also predicted by Density

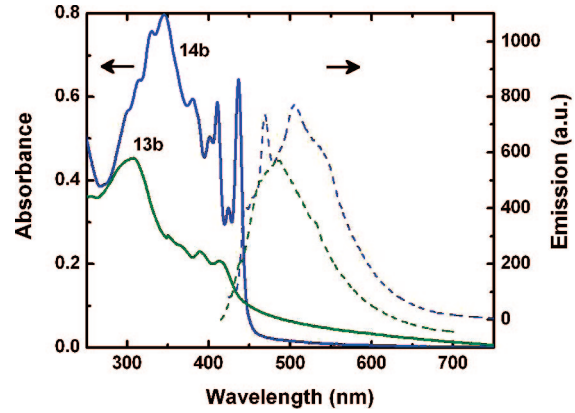

Figure 3. Absorption (solid line) and emission (dotted line) spectra of drop-cast films of **13b** (green line) and **14b** (blue line).

Functional Theory (DFT) calculations showing lower HOMO–LUMO gaps for **14** and supported by experimental observations (Table 1).

All four compounds show strong sky-blue fluorescence in solution, which is also observed in the solid state in the blue region of the visible spectrum (Table 1). The trends noted in the absorption spectra were also observed in the emission spectra with bathochromic shifts between **13** and **14** as well as between the respective unsubstituted (R = H) and substituted (R = hexyl) derivatives. Furthermore, increased photoluminescence quantum yields were obtained for **14** vs **13**. The Stokes shifts of the fluorescence band were rather low and they were lower for the isomer **14** (0.03–0.05 eV) than for the isomer **13** (0.12–0.16 eV), which is in agreement with the longer effective conjugation in **14**. These numbers compare very favorably to typically large Stoke shifts of linear oligothiophenes (0.61 eV for quaterthiophene)[34] and even fused thienoacenes (0.28 eV for pentathienoacene),[34] although even lower Stoke shifts are observed for homoacenes (0.02 eV for anthracene under the same conditions). The low Stokes shifts are indicative of a small structural difference between the excited and ground states and also strongly suggest that the reorganization energy of the charge carrier (polaron or radical cation), which limits the intrinsic mobility of organic semiconductors, will be low.

The photophysical properties of drop-cast films of **13b** and **14b** were investigated and compared with that in solution. As expected, the absorption and emission spectra are bathochromically shifted (by 9 nm for absorption and by 64–69 nm for emission). Also, the peaks become more broad and the vibronic structure is almost completely lost (Figure 3).

X-Ray Crystallography. Long-range molecular ordering is of paramount importance to obtain high charge mobilities in OSCs. In particular, the amount of π-orbital overlap is expected to have a strong influence on the mobility, as has been recently illustrated in structurally related pentacene derivatives.[35] To shed light on supramolecular organization, the crystal structures of **13a** and **14a** have been determined

(32) (a) Jensen, B. S.; Parker, V. D. *J. Am. Chem. Soc.* **1975**, *97*, 5211. (b) Rainis, A.; Swarz, M. *J. Am. Chem. Soc.* **1974**, *96*, 3008.
(33) (a) Houk, K. N.; Lee, P. S.; Nendel, M. *J. Org. Chem.* **2001**, *66*, 5107. (b) Bendikov, M.; Duong, H. M.; Starkey, K.; Houk, K. N.; Carter, E. A.; Wudl, F. *J. Am. Chem. Soc.* **2004**, *126*, 7416.
(34) Zhang, X.; Matzger, A. J. *J. Org. Chem.* **2003**, *98*, 9813.
(35) Sheraw, C. D.; Jackson, T. N.; Eaton, D. L.; Anthony, J. E. *Adv. Mater.* **2003**, *15*, 2009.

Table 2. Crystal Data and Intermolecular Contacts

	13a	14a
a (Å)	12.3815 (14)	11.2784 (24)
b (Å)	5.2570 (6)	5.0330 (11)
c (Å)	12.7975 (15)	14.3066 (31)
β (deg)	97.753 (2)	92.006 (4)
R, R_w (on F^2)	0.0553, 0.1349	0.0464, 0.1103
S1−S1′ (Å)	3.635 (1)	
S2−S2′ (Å)	3.719 (1)	3.769 (1)
S1−S2′ (Å)	3.773 (1)	
τ (deg)[a]	40.12 (1)	41.79 (1)
δ (Å)[b]	3.388 (3)	3.354 (3)

[a] τ is the tilt angle between the mean molecular plane and the stacking axis. [b] δ is the mean interplanar separation between molecules along the π-stack.

by single crystal X-ray diffraction (Table 2). Crystals of **13a** and **14a** both belong to the monoclinic space group $P2_1/n$ and consist of slipped π-stacks (along y) which are aligned into herringbone arrays running along the z-direction. The molecules are completely planar despite the slight steric strain due to interaction between the hydrogen of the central anthracene ring with the hydrogen of the thiophene (2.30 Å for **13a** and with sulfur 2.80 Å for **14a**). Two views of the crystal structure, showing the unit-cell packing and the π-stacked structures, are provided in Figure 4. Such packing is similar to that found in most linear (hetero)acenes and their derivatives. However, the "wider" conjugation framework of **13a** and **14a** still provides for close $\pi\cdots\pi$ contacts (3.388(3) Å and 3.354(3) Å, respectively) within the slipped stack. Moreover, for compound **13a** the intermolecular interaction within these π-stacked arrays and between the stacks is reinforced by close intermolecular S···S contacts (3.635(1), 3.719(1), and 3.773(1) Å). Among these, only one contact (3.635 Å) is slightly lower than double the van-der-Waals radius of sulfur (3.68 Å).[36] The only S···S contacts observed in the crystal structure of **14a** was 3.769 (1) Å. We were not successful in growing quality single crystals of the hexylated molecules **13b** and **14b**. However, considering that the sulfur atoms in the isomer **13** are more exposed than in **14** (where they are almost buried inside the molecule) one could expect more (if any) intermolecular S···S contacts in the hexylated isomer **13b** as compared to **14b**.

Scanning Tunneling Microscopy (STM). While the single-crystal structures of **13a** and **14a** show favorable intermolecular interactions, this does not always lead to high charge mobility in thin film form because the morphology and even the packing of molecules in thin films is often different compared to single crystals. The intermolecular forces in such materials can be quite different at the interface with a substrate and a variety of structures may be observed for organic semiconductors.[37] A famous example is tetraphenyltetracene (rubrene), which shows a planar structure and very high mobility ($\sim$15 $cm^2\ V^{-1}\ cm^{-1}$) in single crystals,[38] but in monolayers on metallic and oxide surfaces adopts a twisted geometry[39] and consequently fails to show any appreciable mobility in thin films. To elucidate the molecular packing on a surface, monolayers of both isomers have been formed by applying solutions of **13b** and **14b** onto highly oriented pyrolytic graphite (HOPG). The formed structures were studied by Scanning Tunneling Microscopy (STM) either at the liquid/solid interface (in octanoic acid) or after drying the solvent (1,2,4-trichlorobenzene), both showing essentially identical structures. Both molecules adsorb on HOPG to form highly ordered self-assembled molecular networks with rectangular unit cells (Figure 5). The difference in unit cell parameters (a = 18.9 Å, b = 21.1 Å, γ = 59.9° for **13b**, and 16.3 Å, 21.5 Å, 65.7° for **14b**) reflects the slightly different orientations of the alkyl chains in the two isomers. According to DFT calculations (B3LYP/6–31G(d)), depending on the torsional angle C−C−C−S in the hexyl chain (0 or 180°), in the gas phase the molecules can exist in two different symmetric (D_{2h}) conformations, *H* and *X* (the letters shape resemble the actual orientation of the alkyl chains in the molecule), which are close in energy (*X* is more stable than *H* by 4.75 kcal/mol for both **13b** and **14b**). Placing the DFT-optimized molecular structures of *X* isomers of **13b** and **14b** in 2D space, in an orientation providing the maximum van der Waals interaction (H···H distances of 2.4 Å) gave periodic structures with excellent resemblance to the contrast of STM images (Figure 5). The same exercise performed with the conformations *H* showed a significantly looser packing (because interdigitation is not possible) with very different periodicities, thus confirming the assembly in the conformation *X*.

Fabrication of Thin-Film Transistors. OTFTs were prepared in bottom-contact configuration by vacuum deposition and drop-casting from chlorobenzene solution. The unsubstituted tetrathienoanthracene **13a** showed no transistor behavior, presumably because of the poor quality of the films. However, pronounced hole mobilities were found for the hexylated derivatives **13b** and **14b**, in both vacuum-deposited and solution-cast films. The transistor output and transfer characteristics are shown in Figure 6 and the obtained data are summarized in Table 3. Keeping the substrate temperature at 75 °C during the deposition improved the order in the films, resulting in a substantial increase of the hole mobility (one to two orders of magnitude). For solution processed films, an increased order can be achieved by rapid (several seconds) heating to the melting point. Although the thus-prepared films are quite rough, even upon optical microscopy inspection, they are also highly crystalline (see XRD in the Supporting Information).

For drop-cast devices, the best hole mobilities (measured at saturation) were 3.5×10^{-3} $cm^2\ V^{-1}\ s^{-1}$ for **13b** and 2.5×10^{-4} $cm^2\ V^{-1}\ s^{-1}$ for **14b**, with an on–off ratio of 1×10^4 for both. As expected, vacuum-deposited films reveal substantially higher mobilities of 7.4×10^{-2} and 1.9×10^{-2} $cm^2\ V^{-1}\ s^{-1}$, for **13b** and **14b**, respectively. While the mobilities of $\leq 1 \times 10^{-1}$ $cm^2\ V^{-1}\ s^{-1}$ are certainly far from the champion values observed in OSCs, the on–off ratio

(36) Zefirovz, Yu. V.; Zorkii, P. M. *Zh. Strukt. Khim.* **1976**, *17*, 745.
(37) (a) Käfer, D.; Ruppel, L.; Witte, G.; Wöll, C. *Phys. Rev. Lett.* **2005**, *95*, 166602. (b) Käfer, D.; Witte, G. *Phys. Chem. Chem. Phys.* **2005**, *7*, 2850. (c) Käfer, D.; Witte, G.; Wöll, C. *J. Mater. Res.* **2004**, *19*, 1889.
(38) Sundar, V. C.; Zaumseil, J.; Podzorov, V.; Menard, E.; Willett, R. L.; Someya, T.; Gershenson, M. E.; Rogers, J. A. *Science* **2004**, *303*, 1644.
(39) (a) Blüm, M. C.; Æavar, E.; Pivetta, M.; Patthey, F.; Schneider, W. D. *Angew. Chem., Int. Ed.* **2005**, *44*, 5334. (b) Cicoira, F.; Miwa, J. A.; Perepichka, D. F.; Rosei, F. *J. Phys. Chem. A* **2007**, in press.

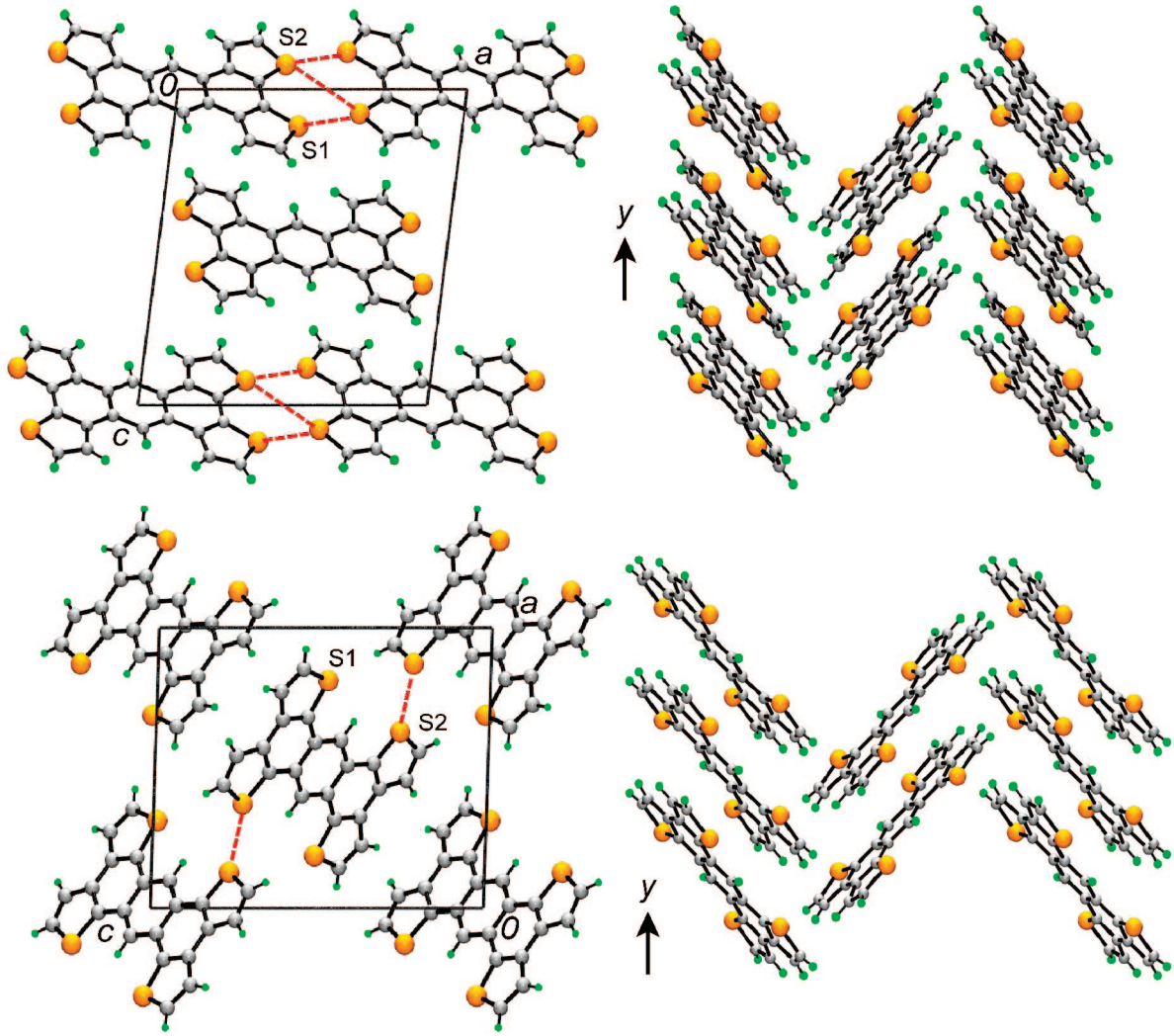

Figure 4. Unit cell (left) and slipped π-stack (right) drawings of **13a** (top) and **14a** (bottom). Intermolecular S···S′ contacts are defined in Table 2.

observed for vacuum-deposited **13b** (1×10^8) is very remarkable. We also note that these are unoptimized values for mobilities. Pentacene OTFTs prepared under identical conditions show a mobility of $\sim 2 \times 10^{-1}$ cm^2 V^{-1} s^{-1} and we fully expect that higher mobility values can be obtained upon device optimization (top-contact configuration, optimized deposition conditions, SiO_2 modification with organic monolayers, etc.). Importantly, in both solution-processed and vacuum-deposited films, isomer **13b** showed higher hole mobility than **14b**. Although detailed structural/morphological analysis of the films is needed to establish the reason for this difference beyond doubts, we note that this difference is in line with higher thermodynamic stability of the radical cation (polaron) of **13b**, but in contrast with the lower reorganization energy (Stoke shift) and HOMO–LUMO gaps of **14b**.

Conclusions

We have developed a synthetic route to a new class of thienoacene derivatives with 2D conjugation pattern. The tetrathienoanthracene structure can be used as a convenient building block to access a variety of related semiconducting molecules through substitution at the thiophene α-position. The two synthesized tetrathienoanthracene regioisomers, **13** and **14**, and their long-chain-substituted derivatives have been characterized by TGA, cyclic voltammetry, UV–vis and fluorescence spectroscopy, X-ray crystallography, and scanning tunneling miscroscopy (STM). From these studies, we conclude that there is an enhancement in the effective conjugation length of isomer **14** over **13** as evidenced by the bathochromic shift and reduced oxidation potential, which was also supported by DFT calculations. TGA results reveal an exceptional thermal stability of these compounds in air ($T_{dec} \approx 400$ °C). X-ray crystallographic studies on parent compounds **13a** and **14a** reveal a slipped π-stacked structure with several close S···S contacts for **13a** (which are less pronounced in **14a**). STM studies of their hexylated derivaties **13b** and **14b** elucidated packing of the molecules in monolayers, which are characterized by a rectangular unit cell, forming a highly oriented two-dimensional structure held together by interactions between the interdigitated hexyl chains. Preliminary studies of OTFT devices in bottom contact configuration showed unoptimized mobilities of up to 0.074 cm^2 V^{-1} s^{-1} and on/off ratio of up to 1×10^8. The isomer **13b** showed higher mobilities than isomer **14b**, regardless of the device preparation method. Although these mobility values are

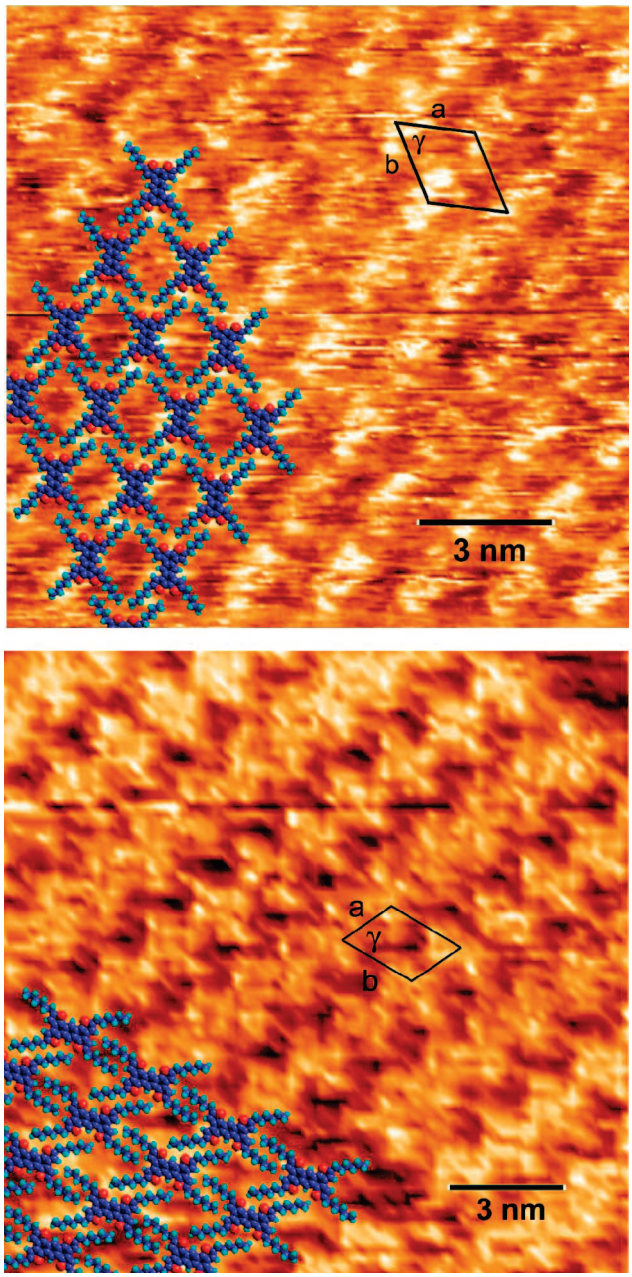

Figure 5. STM image of **13b** (top) from saturated octanoic acid solution and **14b** (bottom) formed from slow evaporation of a 1,2,4-trichlorobenzene solution on HOPG with molecular model. Tunneling current and tip voltage are 300 pA and 800 mV, respectively.

far from the best devices obtained with thienoacene OSCs, they are likely to be improved upon device optimization. Overall, our studies demonstrate that 2D extension of the conjugation through ring fusion is a viable approach to design novel OSCs with very high stability.

Experimental Section

General Procedures and Starting Materials. The reagents *n*-butyllithium (2.0 or 2.9 M in hexanes), *tert*-butyllithium (1.7 M in pentane), tetramethylethylenediamine, diphenyl ether, 3-bromothiophene (Alfa Aesar), tributyltin chloride, 1,2,4,5-tetrabromobenzene, palladium (II) chloride (Alfa Aesar), triphenylphosphine, iron(III) chloride, 2-(tributylstannyl)thiophene, thiophene, diisopropylamine, 1-iodohexane, and *N*-bromosuccinimide were obtained commercially (all from Aldrich except where noted) and used as received. All solvents were of at least reagent grade; diethyl ether and THF were dried by distillation from sodium. All reactions were performed under an atmosphere of dry nitrogen. Melting points are uncorrected. Infrared spectra were run on a Nicolet 6700 FT-IR spectrometer. ^{1}H NMR spectra were run on a Varian Mercury 300 or 400 MHz NMR spectrometer. Low-resolution mass spectra (70 eV, EI and ESI) were run on a Kratos 7525 RFA or Finnigan LCQ DUO mass spectrometer. UV–vis spectra were measured with a Varian Cary 300 or 5000 spectrometer, in 1 cm cuvettes. Fluorescence spectra were measured with a Varian Eclipse spectrofluorometer, in 1 cm cuvettes (in solution) or in drop-cast films on microscope glass and quartz substrates. Thermal gravimetric analysis (TGA) was conducted on a TA Instruments TGA Q500 (temperature rate 20 °C min^{-1} under N_2 and air).

Electrochemistry. Cyclic voltammetry and differential pulse voltammetry were performed on a BAS Epsilon potentiostat in a three-electrode cell in DCM solution of 0.1 M *n*-Bu_4NPF_6 at scan rates of 100 mV s^{-1}. Pt disk and Pt wire were used as the working and counter electrodes, respectively, and a Ag/AgCl electrode was used as the reference.

Crystal Growth. Both **13a** and **14a** were purified by zone sublimation at 1×10^{-4} Torr along a temperature gradient of 240–180–120 °C using an ATS series 3210 three-zone tube furnace, mounted horizontally, and linked to a series 1400 temperature control system. The crystals of **13a** so obtained were suitable for X-ray work. Crystals of **14a** were grown by slow cooling of a saturated benzonitrile solution from 180 to 140 °C.

X-ray Measurements. A needle of **13a** and **14a** was mounted on a nylon loop with paratone. X-ray data were collected at 100 K using omega scans with a Bruker APEX I CCD detector on a D8 3-circle goniometer and Mo Kα (λ = 0.71073 Å) radiation. The data were scanned using Bruker's SMART program and integrated using Bruker's SAINT software.[40] The structure was solved by direct methods using SHELXS-90[41] and refined by least-squares methods on F^2 using SHELXL-97[42] incorporated in the SHELXTL[43] suite of programs.

Scanning Tunneling Microscopy. STM images were acquired from the topography channel of a NanoSurf EasyScan 2, operating at ambient conditions. Tips were mechanically formed from 80/20 PtIr wire (Goodfellow Corporation) and the substrate graphite (SPI-2) was obtained from SPI Supplies. Calibration of the piezoelectric positioner was verified by atomically resolved imaging of graphite. Prior to every experiment, the HOPG substrate was cleaved and the fresh surface was imaged by STM. A saturated solution of **13b** in octanoic acid was introduced between the tip and surface by releasing one drop via pipet. The self-assembled supramolecular nanopattern of **14b**was prepared on the surface of HOPG by releasing one drop of a concentrated trichlorobenzene solution and waiting 24 h until dry. All images have been flattened and lattice-corrected for distortion due to the drift, using WSxM software.[44] Molecular model geometry optimizations were performed at the DFT (B3LYP) level of theory with 6–31G(d) basis set, using the D.01 revision of the Guassian 03W program package.[45]

(40) *SAINT*, version 6.22; Bruker Advanced X-ray Solutions, Inc.: Madison, WI, 2001.
(41) Sheldrick, G. M. SHELXS-90. *Acta Crystallogr., Sect. A* **1990**, *46*, 467.
(42) Sheldrick, G. M. *SHELXL-97. Program for the Refinement of Crystal Structures*; University of Gottingen, Gottingen, Germany, 1997.
(43) *SHELXTL, Program Library for Structure Solution and Molecular Graphics*, version 6.12; Bruker Advanced X-ray Solutions, Inc.: Madison, WI, 2001.
(44) Horcas, I.; Fernandez, R.; Gomez-Rodriguez, J. M.; Colchero, J.; Gomez-Herrero, J.; Baro, A. M. *Rev. Sci. Instrum.* **2007**, *78*, 013705.

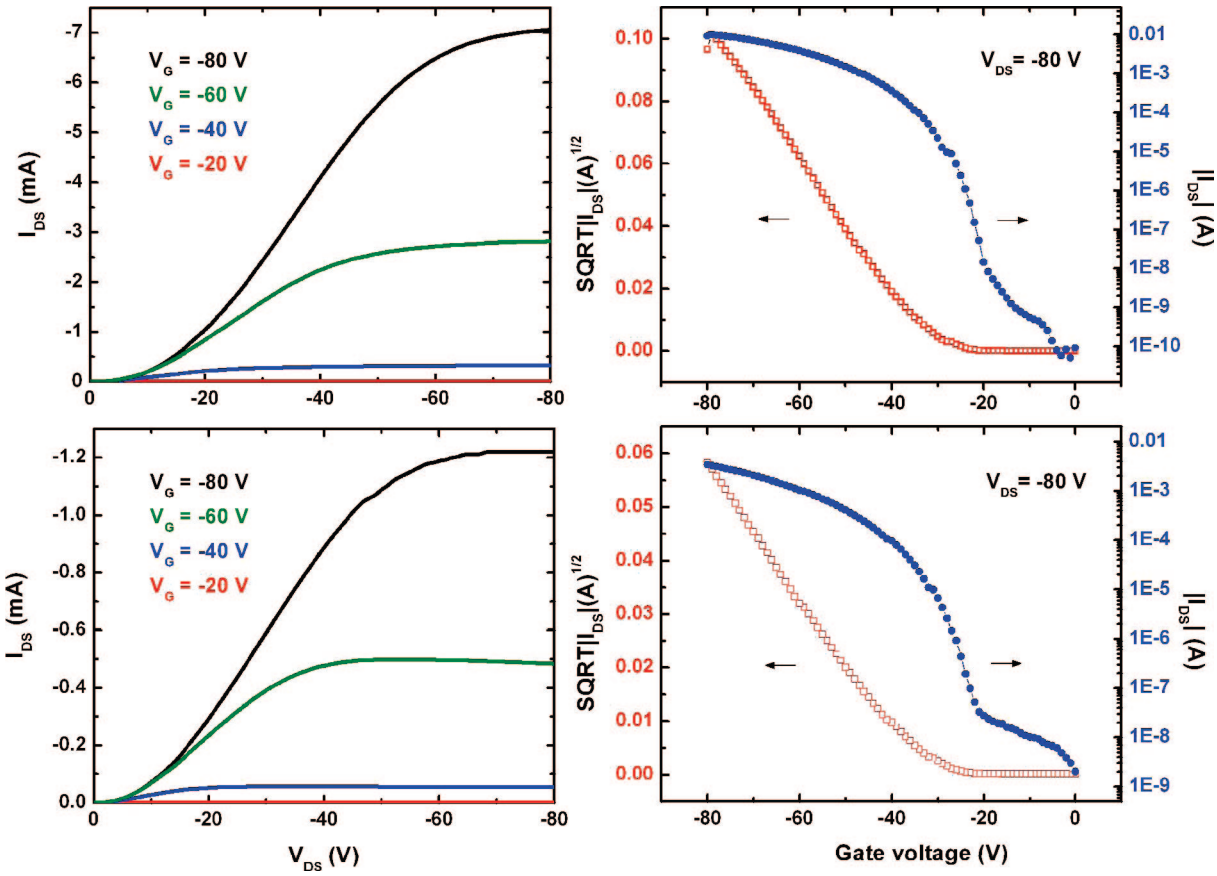

Figure 6. Output (left) and transfer (right) characteristics of compound **13b** (top) and **14b** (bottom) vacuum-sublimed on SiO_2/Si substrates prepatterned with circular Au source and drain electrodes (W/L = 42 000/6 (μm/μm)).

Table 3. FET Characteristics of 13b and 14b

	drop-cast[a]			vacuum-sublimed[b]		
	μ_h ($cm^2\ V^{-1}\ s^{-1}$)	on/off	V_T (V)	μ_h ($cm^2 V^{-1}\ s^{-1}$)	on/off	V_T (V)
13b	3.5×10^{-3}	1×10^4	−18	7.4×10^{-2}	1×10^8	−33
14b	2.5×10^{-4}	1×10^4	−25	1.9×10^{-2}	1×10^6	−30

[a] Annealed as described above. [b] Evaporated on a substrate kept at 75 °C.

Fabrication of Thin-Film Transistors. OTFTs were fabricated, using either interdigitated or single channel circular Au source/drain electrodes (bottom-contact) patterned on 190 nm-thick SiO_2 thermally grown on heavily *n*-doped (Sb, ρ = 0.01–0.02 Ohm cm). The thickness of the electrodes was 25 nm. Au patterning was achieved by lift off using a 5 nm thick Cr adhesion layer. Prior to deposition, substrates were cleaned by sonication in acetone and isopropyl alcohol followed by exposure to O_2 plasma. The interdigitated devices had channel lengths of 6, 10 and 40 μm and corresponding widths of 42 000, 41 000, and 18 000 μm and the single channel devices had channel lengths of 6, 10, 20, and 40 μm and width of 1880 μm. Both interdigitated and single channel devices showed very similar mobilities measured under ambient conditions. OSC films were deposited by either vacuum sublimation with a home-built evaporator (ultimate pressure ~5×10^{-5} Torr) at deposition rates ranging between 0.2 and 1 Å s^{-1} until a thickness of 50 nm was reached, or by drop-casting a concentrated solution of **13b** and **14b** in chlorobenzene on the substrate.

Trithieno[2′,3′:3,4:2′,3′:7,8:3′,2′:5,6]anthra[2,1-*b*]thiophene (13a). A solution of iron (III) chloride (2.13 g, 13.1 mmol) in nitromethane (50 mL) was added dropwise to a solution of **16a** (1.27 g, 3.12 mmol) in DCM (100 mL). ***Caution!*** *Nitromethane is an explosive liquid, which can detonate upon extreme heat. Its contact with amines, alkali metals, and strong reducing agents should be strictly avoided.* After 15 min, methanol (300 mL) was added and the reaction was stirred for 1 h. The product was collected by filtration and rinsed with methanol (1.36 g, 3.38 mmol, 100%). Purification from vacuum sublimation (0.05 mbar, 310 °C) afforded the title compound **13a** as a yellow crystalline solid (136 mg, 10%). Mp: >350 °C (dec). ^{1}H NMR (δ, $CDCl_3$): 9.35 (2H, s), 8.23 (4H, d, J = 5.2 Hz), 7.61 (4H, d, J = 5.2 Hz). IRν_{max} = 3098 (w), 2926 (w), 1317 (w), 1305 (w), 1268 (vw), 1215 (w), 1107 (m), 1094 (w), 911 (m), 866 (s), 812 (m), 710 (vs), 627 (s), 509 (w), 467 (m), 433 (w) cm^{-1}. UV–vis (DCM): λ = 378 nm. MS (EI): *m/z*: 402 (M^+, 100%). Anal. Calcd for $C_{22}H_{10}S_4$: C, 65.64; H, 2.50%. Found: C, 65.75; H, 0.91%. (see the Supporting Information for the clean NMR spectrum).

(45) Frisch, M. J.; Trucks, G. W.; Schlegel, H. B.; Scuseria, G. E.; Robb, M. A.; Cheeseman, J. R.; Montgomery, Jr, J. A.; Vreven, T.; Kudin, K. N.; Burant, J. C.; Millam, J. M.; Iyengar, S. S.; Tomasi, J.; Barone, V.; Mennucci, B.; Cossi, M.; Scalmani, G.; Rega, N.; Petersson, G. A.; Nakatsuji, H.; Hada, M.; Ehara, M.; Toyota, K.; Fukuda, R.; Hasegawa, J.; Ishida, M.; Nakajima, T.; Honda, Y.; Kitao, O.; Nakai, H.; Klene, M.; Li, X.; Knox, J. E.; Hratchian, H. P.; Cross, J. B.; Adamo, C.; Jaramillo, J.; Gomperts, R.; Stratmann, R. E.; Yazyev, O.; Austin, A. J.; Cammi, R.; Pomelli, C.; Ochterski, J. W.; Ayala, P. Y.; Morokuma, K.; Voth, G. A.; Salvador, P.; Dannenberg, J. J.; Zakrzewski, V. G.; Dapprich, S.; Daniels, A. D.; Strain, M. C.; Farkas, O.; Malick, D. K.; Rabuck, A. D.; Raghavachari, K.; Foresman, J. B.; Ortiz, J. V.; Cui, Q.; Baboul, A. B.; Clifford, S.; Cioslowski, J.; Stefanov, B. B.; Liu, G.; Liashenko, A.; Piskorz, P.; Komaromi, I.; Martin, R. L.; Fox, D. J.; Keith, T.; Al-Laham, M. A.; Peng, C. Y.; Nanayakkara, A.; Challacombe, M.; Gill, P. M. W.; Johnsom, B.; Chem, W.; Wong, M. W.; Gonzalez, C.; Pople, J. A. *Gaussian 03, Revision D.01*; Gaussian, Inc.: Pittsburgh, PA, 2003.

2,5,9,12-Tetrahexyltrithieno[2′,3′:3,4:2′,3′:7,8:3′,2′:5,6]anthra[2,1-b]thiophene (13b). A solution of iron(III) chloride (1.1 g, 6.78 mmol) in nitromethane (20 mL) was added dropwise to a solution of **16b** (992 mg, 1.33 mmol) in DCM (50 mL). After 30 min, methanol (300 mL) was added and the reaction was stirred for 45 min. The product was collected by filtration and rinsed with methanol (895 mg, 1.22 mmol, 91%). Column chromatography (9:1 hexanes/ethyl acetate) followed by recrystallization from 1:1 dichloroethane/acetonitrile gave **13b** as a yellow microcrystalline solid (280 mg, 28%). Mp: 215–220 °C. ^{1}H NMR (δ, $CDCl_3$): 9.14 (2H, s), 7.87 (4H, s), 3.06 (8H, t, $J = 7.5$ Hz), 1.87 (8H, q, $J = 7.2$ Hz), 1.20–1.50 (24H, m), 0.92 (12H, t, $J = 6.9$ Hz). ^{13}C NMR (δ, $CDCl_3$): 144.327, 133.741, 130.755, 125.761, 120.123, 119.197, 31.942, 31.908, 31.111, 29.138, 22.862, 14.381. IRν_{max} = 2952 (m), 2924 (s), 2849 (s), 1464 (m), 1454 (m), 1427 (w), 1375 (w), 1318 (w), 1101 (w), 951 (w), 866 (m), 818 (s), 722 (m), 553 (w), 499 (m), 481 (w) cm^{-1}. UV–vis (DCM): $\lambda = 405$ nm. MS (ESI): *m/z*: 739 ([M + H]$^+$; 100%), Anal. Calcd for $C_{46}H_{58}S_4$: C, 74.74; H, 7.91%. Found: C, 73.47; H, 7.76%. (see the Supporting Information for the clean NMR spectrum).

Trithieno[2′,3′:5,6:3′,2′:3,4:3′,2′:7,8]anthra[1,2-b]thiophene (14a). *tert*-Butyllithium (1.0 mL, 1.7 M in pentane, 1.7 mmol) and TMEDA (0.6 mL, 3.98 mmol) were added to a stirring slurry of **14c** (200 mg, 0.278 mmol) in diphenyl ether (50 mL) at 50 °C. ***Caution!*** *Tert-Butyllithium solution is pyrophoric when exposed to air. Transfer of substantial (more than few milliliters) quantities of this material should be done with help of a cannula under nitrogen.* After the solution was stirred for 16 h at 80 °C, more *tert*-butyllithium (1.0 mL, 1.7 M in pentane, 1.7 mmol) and TMEDA (0.6 mL, 3.98 mmol) were added and the reaction mixture was left to stir another 3 h at 80 °C before cooling and quenching with isopropanol. The resulting precipitate was filtered, rinsed with methanol, washed in acetone, and dried in air, affording the title compound **14a** (103 mg, 92%). Purification by vaccum sublimation (0.05 mbar, 300 °C) gave the product as a yellow crystalline solid (45 mg, 0.112 mmol, 44%). UV–vis (DCM): $\lambda = 419$ nm. MS (EI): *m/z*: 402 (M$^+$, 100%). Mp: > 350 °C (dec). ^{1}H NMR (δ, $CDCl_3$): 8.82 (2H, s), 7.46 (4H, d, $J = 5.6$ Hz), 7.29 (4H, $J = 5.2$ Hz). Anal. Calcd for $C_{22}H_{10}S_4$: C, 65.64; H, 2.50; S, 31.86%. Found: C, 65.56; H, 0.00; S, 31.48%. (see the Supporting Information for the clean NMR spectrum).

2,5,9,12-Tetrahexyltrithieno[2′,3′:5,6:3′,2′:3,4:3′,2′:7,8]anthra[1,2-b]thiophene (14b). A solution of iron(III) chloride (953 mg, 5.88 mmol) in nitromethane (20 mL) was added dropwise to a solution of **19b** (1.0 g, 1.35 mmol) in DCM (50 mL). After 30 min, methanol (300 mL) was added and the reaction was stirred for 30 min. The product was collected by filtration and rinsed with methanol, (675 mg, 0.92 mmol, 68%). Recrystallization from 1:1 dichloroethane/acetonitrile afforded **14b** as a yellow crystalline solid (503 mg, 74.6%). Mp: 288–291 °C. ^{1}H NMR (δ, $CDCl_3$): 8.69 (2H, s), 7.36 (4H, s), 3.04 (8H, t, $J = 7.2$ Hz), 1.85 (8H, m), 1.2–1.6 (24H, m), 0.92 (12H, t, $J = 6.6$ Hz).^{13}C NMR (δ, $CDCl_3$): 146.300, 136.120, 133.483, 125.204, 120.260, 118.097, 31.946, 31.794, 31.092, 29.164, 22.892, 14.408. IRν_{max} = 2955 (m), 2922 (vs), 2852 (s), 1553 (w), 1521 (m), 1456 (m), 1432 (s), 1377 (w), 1273 (w), 1119 (w), 1046 (vw), 964 (m), 890 (vw), 856 (s), 835 (vs), 819 (vs), 724 (w), 677 (w), 622 (m), 564 (m), 509 (w) cm^{-1}. UV–vis (DCM): $\lambda = 428$ nm. MS (ESI): *m/z*: 739 ([M+H]$^+$,100%). Anal. Calcd for $C_{46}H_{58}S_4$: C, 74.74; H, 7.91. Found: C, 74.01; H, 7.70. (see the Supporting Information for the clean NMR spectrum).

2,5,9,12-Tetrabromotrithieno[2′,3′:5,6:3′,2′:3,4:3′,2′:7,8]anthra[1,2-b]thiophene (14c). A solution of iron(III) chloride (1.5 g, 9.24 mmol) in nitromethane (25 mL) was added dropwise to a solution of **19c** (1.08 g, 1.50 mmol) in warm chlorobenzene (50 mL), and the reaction mixture was stirred for 30–60 min. The resulting yellow precipitate was filtered, rinsed with DCM, and dried in air. The solid was then stirred in 10% HCl/H_2O for 15 min, filtered, combined with hot methanol (200 mL), filtered, rinsed with methanol, and dried in air to give crude **14c** as a yellow solid (1.07 g, 1.48 mmol, 100%), which was used without further purification. Mp: >350 °C (dec). UV: $\lambda_{max} = 340$ nm (broad). MS (EI): *m/z*: 718 (M$^+$, 52%).

3-[2,4,5-Tris(3-thienyl)phenyl]thiophene (16a). 1,2,4,5-Tetrabromobenzene (2.02 g, 5.14 mmol), palladium(II) chloride (65 mg, 0.367 mmol), triphenylphosphine (195 mg, 0.743 mmol), and 3-(tributylstannyl)thiophene **15** (15.0 g, 40.2 mmol) were stirred at 130 °C in DMF (1 mL) for 16 h. After being cooled to room temperature, the reaction mixture was filtered and the product (1.78 g, 4.47 mmol, 86%) rinsed with hexane. Recrystallization from ethyl acetate afforded clear colorless needles of **16a** (1.62 g, 90%), mp: 350–354 °C. ^{1}H NMR (δ, $CDCl_3$): 7.57 (2H, s), 7.21 (4H, dd, $J_1 = 3.0$ Hz, $J_2 = 2.0$ Hz), 7.13 (4H, dd, $J_1 = 1.2$ Hz, $J_2 = 1.8$ Hz), 6.85 (4H, dd, $J_1 = 1.2$ Hz, $J_2 = 3.9$ Hz). IRν_{max} = 3095 (w), 1541 (vw), 1478 (w), 1426 (vw), 1360 (w), 1319 (w), 1194 (w), 1168 (w), 1078 (m), 905 (w), 886 (w), 854 (m), 781 (s), 748 (m), 728 (w), 675 (s), 625 (m).UV–vis (DCM): $\lambda = 264$ nm.

2-Hexyl-4-[2,4,5-tris(5-hexyl-3-thienyl)phenyl]thiophene (16b). 1,2,4,5-Tetrabromobenzene (100 mg, 0.254 mmol), palladium(II) chloride (8.6 mg, 0.048 mmol), triphenylphosphine (25.8 mg, 0.098 mmol), and **23** (690 mg, 1.51 mmol) were stirred at 130 °C in DMF (1.0 mL) for 24 h. The reaction mixture was cooled, dissolved in DCM and filtered. The filtrate was washed with aqueous NaF (3 × 25 mL), aqueous NaCl (3 × 25 mL), and water (3 × 25 mL). The organic phase was then dried over magnesium sulfate and the solvent was removed. Purification by column chromatography on silica gel with hexanes afforded **16b** (185 mg, 98%) as a pale yellow oil. ^{1}H NMR (δ, $CDCl_3$): 7.50 (2H, s), 6.88 (4H, s), 6.52 (4H, s), 2.70 (8H, t, $J = 7.4$ Hz), 1.23–1.75 (32H, m), 0.92 (12H, t, $J = 7.2$ Hz).

2-[2,4,5-Tris(2-thienyl)phenyl]thiophene (19a). 1,2,4,5-tetrabromobenzene (10.0 g, 25.3 mmol), palladium(II) chloride (320 mg, 1.80 mmol), triphenylphosphine (950 mg, 3.62 mmol), and 2-(tributylstannyl)thiophene **18** (41.0 mL, 129 mmol) were stirred at 130 °C in DMF (5 mL) for 16 h. After being cooled to room temperature, the reaction mixture was filtered and the product (10.14 g, 25.5 mmol, 99%) rinsed with hexane. Recrystallization from ethyl acetate afforded clear colorless needles of **19a** (8.10 g, 80%), mp: 275–280 °C. ^{1}H NMR (δ, $CDCl_3$): 7.66 (2H, s), 7.30 (4H, dd, $J_1 = 1.5$ Hz, $J_2 = 3.3$ Hz), 6.98 (8H, m). IRν_{max} = 3099 (w), 1794 (vw), 1675 (w), 1542 (w), 1441 (w), 1378 (w), 1266 (vw), 1238 (w), 1211 (w), 1079 (w), 1052 (w), 947 (w), 900 (m), 847 (m), 829 (m), 774 (w), 746 (vw), 689 (s), 590 (w), 573 (w), 524 (m), 513 (w). UV–vis (DCM): $\lambda = 287$ nm.

2-(2,4,5-Tris(5-hexyl-2-thienyl)phenyl)-5-hexylthiophene (19b). 1,2,4,5-tetrabromobenzene (5.00 g, 12.7 mmol), palladium(II) chloride (160 mg, 0.902 mmol), triphenylphosphine (475 mg, 1.81 mmol), and **24** (34.17 g, 74.7 mmol) were stirred at 130 °C in DMF (2.5 mL) for 24 h. After being cooled to room temperature, the reaction was dissolved in ether and then washed with aqueous NaF (3 × 50 mL), aqueous NaCl (3 × 50 mL), and water (3 × 50 mL). The organic phase was separated and dried over magnesium sulfate and the solvent was removed to afford the title compound as a dark oil. The product was redissolved in DCM, filtered through a silica plug, concentrated, and cooled to −15 °C to afford **19b** (21.285 g, 100%) as a pale orange crystalline solid, mp: 66–69 °C. ^{1}H NMR (δ, $CDCl_3$): 7.56 (2H, s), 6.74 (4H, d, $J = 3.4$ Hz), 6.62 (4H, d, $J = 3.4$ Hz), 2.76 (8H, t, $J = 7.8$ Hz), 1.63 (8H, m), 1.30 (24H, m), 0.88 (12H, m). IRν_{max} = 2955 (s), 2921 (s), 2871 (m),

2849 (s), 1555 (w), 1504 (m), 1486 (w), 1466 (m), 1377 (m), 1338 (w), 1232 (w), 1210 (vw), 1054 (w), 993 (w), 937 (w), 910 (m), 883 (w), 813 (vs), 798 (vs), 737 (w), 725 (w), 699 (vw), 615 (w), 574 (w), 561 (w), 523 (m) cm^{-1}. UV–vis (DCM): $\lambda_{max} = 299$ nm.

2-Bromo-5-[2,4,5-tris(5-bromo-2-thienyl)phenyl]thiophene (19c). *N*-bromosuccinimide (6.80 g, 38.2 mmol) was added to a solution of **19a** (2.53 g, 6.22 mmol) in THF (125 mL) and stirred at room temperature for 16 h. The resulting white precipitate was filtered, rinsed with acetone, and washed in water before drying in air to give the product **19c** as a white solid (3.37 g, 75%). Mp: 258–262 °C. ^{1}H NMR (δ, $CDCl_3$): 7.50 (2H, s), 6.97 (4H, d, J = 3.6 Hz), 6.73 (4H, d, J = 3.8 Hz). IRν_{max} = 3093 (vw), 1479 (m), 1442 (w), 1421 (w), 1365 (w), 1193 (w), 1023 (w), 976 (m), 965 (m), 929 (w), 905 (m), 866 (w), 790 (s), 698 (w), 661 (w), 583 (m), 509 (m), 431 (m) cm^{-1}. UV–vis (DCM): $\lambda_{max} = 300$ nm. A second crop was obtained from evaporation of the filtrate. The resulting white solid was washed with water, rinsed with acetone, and dried in air (1.12 g, 25%). Spectroscopic data were identical to those reported above.

2-Hexylthiophene (20).[46] *n*-Butyllithium (95 mL, 2.9 M in hexanes, 0.275 mol) was added to a solution of thiophene (20 mL, 0.250 mol) in THF (150 mL) at −78 °C. The temperature was allowed to slowly rise to room temperature and the mixture was stirred for 75 min. Upon the temperature being reduced back to −78 °C, 1-iodohexane (40 mL, 0.275 mol) was added and the reaction was stirred for an additional 16 h before it was filtered, poured over water, and extracted with DCM. The organic phase was separated and dried over magnesium sulfate, and the solvent was removed to afford crude 2-hexylthiophene **20** (42.6 g, 100%). Vacuum distillation (0.6–0.9 mbar, 55 °C) gave the product (35.7 g, 85%) as a reddish oil. ^{1}H NMR (δ, $CDCl_3$): 7.11 (1H, d, J = 5.4 Hz), 6.92 (1H, t, J = 4.5 Hz), 6.78 (1H, d, J = 3.0 Hz), 2.83 (2H, t, J = 7.5 Hz), 1.68 (2H, q, J = 7.2 Hz), 1.35 (6H, m), 0.89 (3H, t, J = 6.0 Hz).

2-Bromo-5-hexylthiophene (21). *N*-Bromosuccinimide (1.95 g, 10.9 mmol) was added to a stirring solution of **20** (1.77 g, 10.5 mmol) in 2:1 chloroform/acetic acid (50 mL) at 0 °C. The mixture was stirred for 16 h at room temperature then poured onto water and extracted with hexanes. The organic phase was separated and dried over magnesium sulfate and the solvent removed to afford crude 5-bromo-2-hexylthiophene **21**[47] (2.52 g, 97%). ^{1}H NMR (δ, $CDCl_3$): 6.83 (1H, d, J = 3.6 Hz), 6.52 (1H, d, J = 3.6 Hz), 2.73 (2H, t, J = 7.2 Hz), 1.62 (2H, q, J = 7.6 Hz), 1.30 (6H, m), 0.88 (3H, t, J = 6.8 Hz).

3-Bromo-5-hexylthiophene (22). *n*-Butyllithium (9.5 mL, 2.5 M in hexanes, 23.7 mmol) was slowly added to a solution of diisopropylamine (4.75 mL, 33.9 mmol) in THF (175 mL) at 0 °C.[31] After 30 min, a solution of **21** (4.86 g, 19.7 mmol) in THF (60 mL) was added; the mixture was stirred at room temperature for 16 h and then poured onto water and extracted with DCM. The organic phase was separated and dried over magnesium sulfate and the solvent was removed to afford crude **22** (4.70 g, 97%). The product was filtered through silica (in hexane) and distilled in vacuum (0.5 mbar, 95 °C) affording pure **22**[48] (3.36 g, 64%) as a pale yellow oil. ^{1}H NMR (δ, $CDCl_3$): 7.00 (1H, s), 6.70 (1H, s), 2.77 (t, 2H, 7.5 Hz), 1.64 (2H, m), 1.30 (6H, m), 0.88 (3H, m).

3-(Tributylstannyl)-5-hexylthiophene (23). *tert*-Butyllithium (6.9 mL, 1.7 M in pentane, 11.7 mmol) was slowly added to a solution of **22** (2.70 g, 10.9 mmol) in anhydrous diethyl ether (8.5 mL) at −78 °C. After being stirred for 5 min, tributyltin chloride (3.2 mL, 11.8 mmol) was slowly added and the mixture was stirred for 24 h at room temperature. The reaction was then poured onto water and extracted with DCM. The organic phase was separated and dried over magnesium sulfate, and the solvent was removed to afford the title compound **23** (5.04 g, 100%) as a pale orange oil which was used without further purification. ^{1}H NMR (δ, $CDCl_3$): 7.08 (s, 1H), 6.76 (s, 1H), 2.84, (t, 2H, J = 7.8 Hz), 0.82–1.77 (38H, m).

2-(Tributylstannyl)-5-hexylthiophene (24). *n*-Butyllithium (36 mL, 2.9 M in hexanes, 0.105 mol) was added to a stirring solution of 2-hexylthiophene **20** (11.8 g, 70 mmol) in anhydrous diethyl ether (30 mL) at −78 °C. The temperature was allowed to slowly rise to room temperature and the reaction mixture was stirred for 24 h. Tributyltin chloride (21 mL, 78 mmol) was added and the mixture was stirred at room temperature for an additional 24 h. The reaction was then poured onto water and extracted with DCM. The organic phase was separated and dried over magnesium sulfate and the solvent was removed to afford the title compound **24**[49] (34.2 g, 100%), which was used without further purification. ^{1}H NMR (δ, $CDCl_3$): 6.98 (d, 1H, J = 3.3 Hz), 6.90 (d, 1H, J = 3.0 Hz), 2.85 (t, 2H, J = 7.5 Hz), 0.68–1.74 (38H, m).

Acknowledgment. The authors thank Oleksandr Ivasenko for his help with STM analysis and Nadim Saade for mass-spectral analysis. We are grateful to NSERC, FQRNT, and the ACS Petroleum Research Fund for funding this work. J.L.B. and D.F.P. acknowledge support through an NSERC postdoctoral fellowship and a DuPont Young Professor award, respectively.

Supporting Information Available: ^{1}H NMR for compounds **13a**, **13b**, **14a**, **14b**, **16a**, **16b**, **19a**−**c** and **20**–**24**; UV–vis and fluorescence spectra for **13a**, **14a**, **16a**, **16b**, **19a**, and **19b** in solution and for **13b** and **14b** in thin films; TGA curves and XRD patterns for **13b** and **14b** (PDF); details of X-ray crystallographic data collection and structure refinement, table of atomic coordinates, bond distances and angles, anisotropic thermal parameters and hydrogen atom positions for **13a** and **14a** (CIF). This material is available free of charge via the Internet at http://pubs.acs.org.

CM7030653

(46) Van Breeman, A. J. J. M.; Herwig, P. T.; Chlon, C. H. T.; Sweelssen, J.; Schoo, H. F. M.; Setayesh, S.; Hardeman, W. M.; Martin, C. A.; de Leeuw, D. M.; Valeton, J. J. P.; Bastiaansen, C. W. M.; Broer, D. J.; Popa-Merticaru, A. R.; Meskers, C. J. *J. Am. Chem. Soc.* **2006**, *128*, 2336.

(47) Barbarella, G.; Favaretto, L.; Sotgiu, G.; Zambianchi, M.; Antolini, L.; Pudova, O.; Bongini, A. *J. Org. Chem.,* **1998**, *63*, 5497.

(48) Chow, K.; Lai, R.; Holmes, J. M.; Wijono, M.; Wheeler, L. A.; Garst, M. E. *Eur. J. Med. Chem.,* **1996**, *31*, 175.

(49) Wilson, P.; Lacey, D.; Sharma, S.; Worthington, B. *Mol. Cryst. Liq. Cryst.* **2001**, *368*, 279.

(50) For each compound and reference standard, six solutions of varying concentration (~0.01–0.1 abs) were prepared with the appropriate solvent (**13a** and **13b**, DPA in DCM; **14a** and **14b**, anthracene in cyclohexane) and plots of fluorescence emission as a function of absorbance (at the excitation wavelength; 370 nm for **13a** and **13b**, and DPA, 324 nm for **14a**, **14b**, and anthracene) generated. Linear regression analysis was performed and the slope for each compound relative to its reference standard was assumed equivalent to its quantum yield.

(51) Hamai, S.; Hirayama, F. *J. Phys. Chem.* **1983**, *87*, 83.

(52) Berlman, I. B. *Handbook of Fluorescence Spectra of Aromatic Molecules*; Academic Press: New York, 1971.